Reconstruction-driven motion estimation for motion-compensated MR CINE imaging

Jiazhen Pan, Wenqi Huang, Daniel Rueckert, Fellow, IEEE, Thomas Küstner[†], Member, IEEE and Kerstin Hammernik[†]

Abstract—In cardiac CINE, motion-compensated MR reconstruction (MCMR) is an effective approach to address highly undersampled acquisitions by incorporating motion information between frames. In this work, we propose a deep learning-based framework to address the MCMR problem efficiently. Contrary to state-of-the-art (SOTA) MCMR methods which break the original problem into two sub-optimization problems, i.e. motion estimation and reconstruction, we formulate this problem as a single entity with one single optimization. We discard the canonical motion-warping loss (similarity measurement between motion-warped images and target images) to estimate the motion, but drive the motion estimation process directly by the final reconstruction performance. The higher reconstruction quality is achieved without using any smoothness loss terms and without iterative processing between motion estimation and reconstruction. Therefore, we avoid non-trivial loss weighting factors tuning and time-consuming iterative processing. Experiments on 43 inhouse acquired 2D CINE datasets indicate that the proposed MCMR framework can deliver artifact-free motion estimation and high-quality MR images even for imaging accelerations up to 20x. The proposed framework is compared to SOTA non-MCMR and MCMR methods and outperforms these methods qualitatively and quantitatively in all applied metrics across all experiments with different acceleration rates.

Index Terms—motion-compensated reconstruction, Cardiac CINE reconstruction, deep learning, reconstruction-driven registration / motion estimation

I. INTRODUCTION

► INE cardiac magnetic resonance imaging (CMR) serves as a versatile tool for characterizing cardiac morphology and assessing cardiac function. Quantitative indicators such as volume and ejection fraction can be calculated from CMR and an evidence-based diagnosis of cardiovascular disease can be accomplished. A reconstruction with high spatial and temporal resolutions across the whole cardiac sequence is an indispensable prerequisite for CMR. In this context, a short scan time, ideally within a single breath-hold, is preferred to alleviate the patients' scan discomfort and prevent potential image

This work was supported in part by the European Research Council (Grant Agreement no. 884622).

† Thomas Küstner and Kerstin Hammernik contributed equally.

Jiazhen Pan, Wenqi Huang, Daniel Rueckert and Kerstin Hammernik are with Klinikum Rechts der Isar, Technical University of Munich, Munich, Germany (e-mail: jiazhen.pan@tum.de; wenqi.huang@tum.de; daniel.rueckert@tum.de; k.hammernik@tum.de).

Thomas Küstner is with the University Hospital of Tuebingen, Department of Diagnostic and Interventional Radiology, Medical Image and Data Analysis (MIDAS.lab), Tübingen, Germany (e-mail: thomas.kuestner@med.uni-

Daniel Rueckert and Kerstin Hammernik are also with the Department of Computing, Imperial College London, London, United Kingdom.

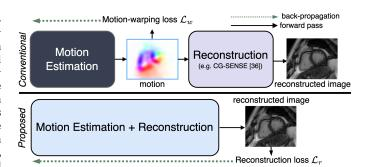


Fig. 1. The difference between the proposed MCMR framework (bottom) and the conventional MCMR work (top) is shown. The conventional approaches divide the original MCMR problem into two sub-optimization problems: motion estimation and reconstruction. Its motion estimation is optimized by minimizing the intermediate motion-warping loss (brightness similarity measurement between motion-warped images and target images) and if deep learning is used, the motion prediction back-propagation is only exerted on the motion estimation part. In contrast, we develop a deep learning-based framework that predicts the motion from the perspective of our ultimate goal: reconstruction. We discard using any intermediate motion-warping loss. The back-propagation is performed through the whole pipeline and reconstructiondriven motion estimation is established.

artifacts due to patient motion. To this aim, only a limited amount of k-space (frequency domain) data can be collected for every temporal frame, violating the Nyquist-Shannon sampling theorem and resulting in aliasing artifacts in the image domain. In the past decade, Parallel Imaging [1], [2] and Compressed Sensing [3], [4] were introduced in CMR, enabling shorter scan time and improved reconstruction performance. However, reconstruction performance can be further improved if adequate spatial-temporal information is shared along the cardiac cycle. This information is linked by the cardiac motion, which bridges every single frame of the whole cardiac sequence and serves as the key to successful reconstruction. A straightforward way to leverage this motion information in CMR reconstruction is to use motion-compensated MR reconstruction (MCMR) [5] in which the cardiac motion has to be estimated. However, precise cardiac motion estimation remains a challenging problem due to the non-rigid nature of the cardiac motion, especially in the case of accelerated imaging where motion has to be estimated from undersampled data.

To circumvent the non-trivial tasks of cardiac motion estimation, different CMR reconstruction methods sidestep the motion estimation and aim to exploit spatio-temporal redundancies. The works of [6], [7] suggested disentangling the original reconstruction problem into a low-rank and a sparse component and these two sub-optimizations are carried out jointly. However, the preservation of dynamic information crucially depends on the optimization of the sparse component and the implementation of soft thresholding can incur information loss. Moreover, deep learning reconstructions were proposed e.g. [8], [9] that unroll the dynamic MR optimization process with a spatio-temporal regularization. In this case, multiple unrolled gradient descent steps have to be executed, giving rise to the training difficulty of the network and processing time in both training and testing. Other methods [10]-[12] utilized the k-t domain to leverage the spatiotemporal redundancies to ameliorate the dynamic reconstruction. Whereas all these methods endeavor to extract the spatiotemporal correlation implicitly, there is no guarantee that the correlation of every cardiac frame is fully exploited. On the contrary, MCMR leverages the estimated cardiac motion to explicitly share cardiac spatio-temporal information.

A high-quality MCMR can be performed if the cardiac motion can be estimated precisely over the whole cardiac cycle. Therefore, the selection of a proper motion estimation/registration approach plays a decisive role in MCMR. Conventional registration methods based on B-spline [13], [14] or diffusion method [15] can be employed as motion estimators in MCMR. These methods can provide meaningful registration results but demand enormous computing time in the order of hours for a single CMR sequence. Furthermore, hyper-parameter tuning for these methods [13], [14] is also a non-trivial task, hindering their implementation in clinical practice. Lately, learning-based registration/motion estimation approaches have been introduced into medical imaging [16]-[18] and embodied in the application of cardiac motion estimation [19]–[21]. These methods accelerate the registration time from hours to seconds by leveraging a trained neural network during inference and mitigating hyper-parameter tuning. However, these cardiac registration methods are not designed for the MCMR context but are designed to minimize the brightness inconsistency of estimated motion-warped images and target images (motion-warping error). Yet in the context of accelerated imaging, the undersampled input images exhibit artifacts and intensity inconsistencies. The direct application of these general motion estimation/registration methods to accelerated imaging data can result in imprecise motion fields and can thus incur error propagation in MCMR. Qi et al. [22] circumvented this problem by providing reference images in the training loss whilst feeding undersampled data as network inputs. Concurrently, a registration method designed for the MCMR context is proposed by Küstner et al. [23] in which the registration is directly estimated from the k-space. All aforementioned methods conduct a pair-wise motion estimation and they have to be carried out multiple times in MCMR, in which for every single frame a registration from multiple other frames is required. To provide a more efficient and time-continuous registration, groupwise motion estimation has been studied [24], [25]. In group-wise registration, the spatialtemporal redundancy over multiple frames can be leveraged to facilitate the registration, especially when through-plane motion occurs in the context of 2D CMR. Furthermore, the temporal coherence over the cardiac cycle can be instilled during training by applying a temporal loss term [24].

After the choice of a proper motion estimation/registration method, there are multiple MCMR frameworks available to combine the motion estimator and reconstruction. The seminal work [5] of Batchelor et al. pioneered the MCMR concept in which the motion information is embedded as a general matrix into the MR forward model. This work formulated the MCMR problem with two individual stages: motion estimation and reconstruction. The motion estimation in the first stage and the reconstruction in the second stage are both carried out separately, while the pre-calculated motion from the first stage is regarded as a fixed matrix in the second-stage reconstruction [22], [26], [27]. Furthermore, MCMR can also be reformulated as a joint optimization problem in which an iterative optimization of image reconstruction and motion estimation are carried out alternatively. A potential synergy can be established: a more accurate motion estimation can provide a better reconstruction, and based on a less artifacts-affected image a better motion estimation can be accomplished. Odille et al. proposed a reconstruction method using sensor-based motion estimation e.g. respiratory belt or ECG signal [28], [29]. The need for external tracking hardware is relieved by adopting B-spline-based and optical flow-based motion estimation in this joint optimization context [30], [31]. More recently, variational methods [32] and dictionary learning [33] are also employed to solve this joint optimization problem for CMR reconstruction. However, all these methods demand a relatively long estimation time because of their iterative optimization nature. Therefore, deep-learning-based methods were proposed to speed up joint optimization. [25], [34] unrolled MCMR joint optimization with a group-wise motion estimation network and the mutual benefit of CMR reconstruction and motion estimation is demonstrated in their work.

However, the decomposition of the MCMR into two suboptimization problems serves as a workaround to solve MCMR has two major drawbacks: First, the solution space of the full problem is restricted by the solution of the motion-estimation problem itself whose goal is to minimize the motion-warping loss between different cardiac frames. This goal is not necessarily aligned with the final reconstruction objective due to undersampled images' artifact-degradation and intensityinconsistency amongst cardiac frames. Second, extra efforts have to be built in to cope with motion estimation in the case of accelerated imaging with undersampled data, e.g. extra preprocessing steps with intra-bin motion correction [26], [27], loss function tuning [22] or k-space motion estimation [35]. Although the estimation difficulty of the motion can be reduced if the alternating joint optimization is used, it requires multiple iterations of motion estimation and reconstruction to yield satisfactory reconstruction, prolonging the processing time. On the contrary, in this work we propose an MCMR framework that optimizes the complete MCMR framework together without breaking it into two sub-optimization problems.

Moreover, all aforementioned MCMR methods follow the suggestions of [5] which applied all temporal frames to reconstruct one single frame of the sequence so that all temporal redundancy can be exploited. We argue in this work that using a smaller amount of temporal frames to conduct the MCMR

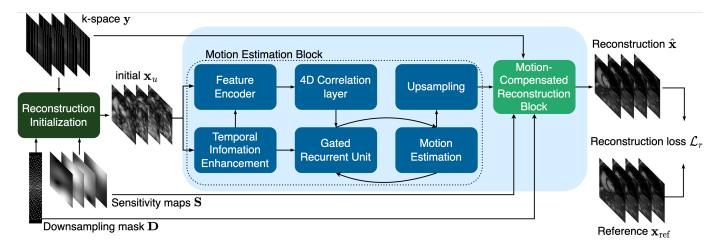


Fig. 2. Architecture of the proposed method: Motion-compensated MR reconstruction (MCMR) framework with a *Motion Estimation Block* (refer to III-A) and a complex-valued *Motion-Compensated Reconstruction Block* (refer to III-B). The motion estimation learning process is directly driven by the final reconstruction performance. A pre-processing reconstruction is implemented (*Reconstruction Initialization*, refer to II-A) prior to the proposed method to alleviate the reconstruction difficulty.

can achieve a better result. This setting reduces the residual motion-warping error from other temporal frames while still leveraging enough redundant information.

In summary, the main contributions of our work are as follows: (a) We propose a deep learning-based approach, which efficiently solves the motion-compensated reconstruction and addresses the MCMR problem as a single entity. Our framework estimates motion from the perspective of CMR reconstruction, rather than motion estimation alone. We establish an efficient mechanism in which the motion estimation process is directly driven by the final reconstruction results (refer to Fig. 1) and without using iterative joint optimization of motion estimation and reconstruction. (b) We investigate the optimal number of temporal frames to use during the MCMR. We observe that using a smaller amount of frames to reconstruct the cardiac frames achieves better performance than using all frames of a sequence. We find a balance between the exploitation of sequence redundancy and the suppression of residual warping error, which can inspire all other MCMR methods. (c) We demonstrated the reconstruction of images from undersampling rates up to 20x with the optimization only depending on one final reconstruction loss term. The canonical motion-warping loss including smoothness terms that serve as an intermediate loss in MCMR is discarded in this work. Therefore, we avoid the non-trivial weighting factor tuning. We applied our method on 43 in-house acquired CMR CINE data and compared it to several canonical and SOTA methods. Our method outperforms the baselines with superior qualitative and quantitative results.

II. PROBLEM FORMULATION

A. General MR Reconstruction

Let $x^{(t)} \in \mathbb{C}^N$ indicate the t-th complex-valued temporal frame of the dynamic CINE sequence $\mathbf{x} = [x^{(1)}, \dots, x^{(T)}]$ stacked as a column vector and N denotes the amount of pixels in the 2D plane, i.e. $N = N_X N_Y$ with X, Y the height and width of the frame and T the number of temporal phases.

 $y^{(t)} \in \mathbb{C}^{SN}$ from $\mathbf{y} = [y^{(1)}, \dots, y^{(T)}]$ is the corresponding undersampled k-space data with S being the number of MR receiver coils. Regarding the CMR reconstruction task of a retrospectively gated CINE, the following inverse problem has to be solved:

$$\min_{x^{(t)}} \left\| \mathbf{A}^{(t)} x^{(t)} - y^{(t)} \right\|_{2}^{2}, \ t = 1, \dots, T.$$
 (1)

 $\mathbf{A}^{(t)}$ represents the MR forward multi-coil encoding operator with $\mathbf{A}^{(t)} = \mathbf{D}^{(t)}\mathbf{F}\mathbf{S}$, in which $\mathbf{S} \in \mathbb{C}^{SN \times N}$ denotes the coil sensitivity maps, $\mathbf{F} \in \mathbb{C}^{SN \times SN}$ is the forward Fourier encoding matrix, $\mathbf{D}^{(t)} \in \mathbb{R}^{SN \times SN}$ is the undersampling mask diagonal matrix. Eq. (1) can be solved by using general conjugate-gradient SENSE (CG-SENSE) [36] reconstruction which is performed T times to reconstruct these T cardiac frames. However, this general MR reconstruction method optimizes every cardiac frame $x^{(t)}$ separately regardless of the adequate temporal information across the cardiac sequence. Therefore, its reconstruction performance is limited with respect to the undersampling ratio. In this work, we use this general CG-SENSE as an initialization step (*Reconstruction Initialization* in Fig. 2) for the following MCMR task.

B. Motion-compensated MR reconstruction with a varying number of input neighboring frames

As mentioned above, leveraging the temporal information in the cardiac sequence can facilitate the CMR reconstruction. The spatial-temporal redundant information is bridged by the cardiac motion. Following the work of Batchelor *et al.* [5], motion is embedded into the MR forward model and information from other temporal frames can be leveraged as complements:

$$\min_{x^{(t)}} \left\| \mathbf{A}^{(K)} \mathbf{U}^{(t \to K)} x^{(t)} - \mathbf{y}^{(K)} \right\|_{2}^{2}, \ t = 1, \dots, T$$
 (2)

where K=2k+1 denotes the neighboring $\pm k$ frames of the frame t. The k-spaces $\mathbf{y}^{(K)}=[y^{(t-k)},\ldots,y^{(t)},\ldots,y^{(t+k)}]\in$

 \mathbb{C}^{SNK} are used as complementary neighboring data to reconstruct the frame $x^{(t)}$. We assume periodicity in the cardiac cycle, i.e. the previous frame to $x^{(0)}$ is regarded as $x^{(T)}$. $\mathbf{U}^{(t \to K)} \in \mathbb{R}^{NK \times N}$ denotes the cardiac motion matrix and warps $x^{(t)}$ to the K cardiac frames. By means of $\mathbf{U}^{(t \to K)}$, the redundancy and correlation of the neighboring cardiac frames of $x^{(t)}$ are instilled for the t-th frame reconstruction. It should be noted that our MCMR framework differs from the original MCMR framework [5] which applied all temporal frames K = T to conduct the reconstruction, while in our case we choose K < T as detailed in Section V-A. Analogously to $\mathbf{A}^{(t)}$, $\mathbf{A}^{(K)} = \mathbf{D}^{(K)}\mathbf{FS} \in \mathbb{C}^{SNK \times NK}$ denotes the CMR forward model for these K frames.

III. METHOD

In this work, we propose a deep-learning-based framework to reconstruct the dynamic CINE images. This framework consists of two parts: a Motion Estimation Block which tries to estimate cardiac motion and a Motion-Compensated Reconstruction Block which is purposed for carrying out the motioncompensated reconstruction, depicted in Fig. 2. In contrast to all the previously proposed MCMR works, our framework can be trained end-to-end which regards the motion estimation and reconstruction processes as a single entity instead of splitting them into two sub-tasks. Furthermore, unrolling the iterative procedure of motion estimation and reconstruction prolongs the processing time and renders itself inefficient. In this work we aim to estimate precise motion directly from the undersampled data by using one-shot prediction with a motion estimator \mathcal{G} and then solve the inverse problem with an ℓ_2 regularizer using the initial sequence \mathbf{x}_u provided by Reconstruction Initialization block, read as:

$$\hat{\mathbf{U}} = \mathcal{G}\left(\mathbf{x}_u\right) \tag{3a}$$

$$\hat{\mathbf{x}} = \arg\min_{\mathbf{x}} \left\| \mathbf{A} \hat{\mathbf{U}} \mathbf{x} - \mathbf{y}^{(TK)} \right\|_{2}^{2} + \lambda \left\| \mathbf{x} - \mathbf{x}_{u} \right\|_{2}^{2}, \quad (3b)$$

where λ presents the weighting factor of the applied ℓ_2 term. $\hat{\mathbf{U}} \in \mathbb{R}^{NTK \times NT}$ denotes the estimated cardiac motion which is used inside the MCMR, $\hat{\mathbf{x}}$ denotes the final reconstructed image for all cardiac frames. $\mathbf{y}^{(TK)} = [y^{(1-k)}, \ldots, y^{(1+k)}, \ldots, y^{(T-k)}, \ldots, y^{(T+k)}]$ extends from $\mathbf{y}^{(K)}$ presenting the adopted complementary neighboring frames to reconstruct every $x^{(t)}$ of the cardiac sequence \mathbf{x} .

A. Motion Estimation Block

We utilize a learning-based motion estimation network \mathcal{G} with trainable parameters θ to predict the non-rigid cardiac motion. The backbone of GRAFT [24] is applied to model \mathcal{G} . GRAFT is a group-wise motion estimation network that takes the undersampled cardiac sequence \mathbf{x}_u as input and predicts the motion between the frames. Its inherent *Temporal Information Enhancement* Block consists of convolutional layers which take the target frame along with its one previous and subsequent cardiac frame as input and extract the spatial-temporal information from them. By means of that, the problem of through-plane motion and occlusion can

be alleviated. Afterward, a Feature Encoder is incorporated which processes the embedding from Temporal Information Enhancement Block and extracts the information from the image sequence. Subsequently, a 4D-Correlation layer is performed to compute the correlation of the 2D spatial plane and a Gated Recurrent Unit (GRU) is employed to conduct an iterative motion estimation. Finally, the motion is upsampled $4\times$ to the original image size. This process is carried out K times and a motion field $\hat{\mathbf{U}}$ mapping from dimension NT to NTK is produced by GRAFT at this end.

warping Usually, a similarity measurement utilized to drive the learning of the motion $\mathcal{L}_w(\mathbf{x}^{(K)}, \hat{\mathbf{U}}^{(t \to K)} x^{(t)})$ network: estimation with $\mathbf{x}^{(K)} = [x^{(t-k)}, \dots, x^{(t)}, \dots, x^{(t+k)}]$ the target frames from \mathbf{x} and $\hat{\mathbf{U}}^{(t\to K)}x^{(t)}$ its corresponding warped estimation. However, \mathcal{L}_w is just an intermediate motion-warping loss function in the context of MCMR. As mentioned in Section I, the loss' effectiveness is undermined by the increase of the undersampling rate (more aliasing and severe intensity inconsistency) whose goal diverges from the goal of improving the final reconstruction quality. Furthermore, the utilization of \mathcal{L}_w after the Motion Estimation Block breaks the original MCMR optimization into two sub-tasks, introducing the drawbacks as mentioned in Section I. In this work, we do not calculate \mathcal{L}_w at this intermediate position but forward the output motion $\hat{\mathbf{U}}$ of \mathcal{G} to the subsequent Motion-Compensated Reconstruction Block. Since no network loss function is applied yet, the motion prediction $\hat{\mathbf{U}}$ with learnable parameters θ are still pending and the complete forward chain of the applied deep learning model is to be established by the subsequent Motion-Compensated Reconstruction Block.

B. Motion-Compensated Reconstruction Block

The *Motion-Compensated Reconstruction Block* is a complex-valued operator which executes the CINE reconstruction and serves as the forward pass for the network prediction $\hat{\mathbf{U}}$ to reach the final loss function. This block solves Eq. (3b) by finding the stationary point utilizing the normal function:

$$\underbrace{\left(\hat{\mathbf{U}}^{H}\mathbf{A}^{H}\mathbf{A}\hat{\mathbf{U}} + \lambda\mathbf{I}\right)}_{\mathcal{V}}\hat{\mathbf{x}} = \underbrace{\left(\hat{\mathbf{U}}^{H}\mathbf{A}^{H}\mathbf{y}^{(TK)} + \lambda\mathbf{x}_{u}\right)}_{\mathbf{h}}.$$
 (4)

Since the inverse of matrix \mathcal{V} is computationally prohibitive to calculate, we adopt Conjugate Gradient (CG) [37] to solve this problem in an iterative manner until the process converges. Therefore, we present the final output of the *Motion-Compensated Reconstruction Block* in the basis of a set of conjugate vectors $\mathcal{P} = \{\mathbf{p}_0, ..., \mathbf{p}_I\}$:

$$\hat{\mathbf{x}} = \sum_{i=0}^{I} \alpha_i \mathcal{V} \mathbf{p}_i. \tag{5}$$

Here, $(\mathbf{p}_i)^H \mathcal{V} \mathbf{p}_j = 0$ for all $i \neq j$ and α_i are their corresponding basis coefficients. In the following we will describe the conjugate gradient algorithm, to comprehend the end-to-end nature of our proposed approach. Details of the applied CG are shown in Alg. 1. \mathbf{p}_i and α_i can be obtained during the iteration

update of CG and I is its predefined total iteration number. All α_i and \mathbf{p}_i are calculated based on \mathcal{V} while \mathcal{V} is computed based on the motion matrix $\hat{\mathbf{U}}$. In contrast to conventional works, it is important to note that $\hat{\mathbf{U}}$ here is not a static fixed matrix but still a pending variable from $\mathcal{G}(\mathbf{x}_u)$. Its trainable parameters θ still wait for updates through back-propagation on a higher-level loss function for network training. To express this more clearly, we reformulate Eq. (5) with Eq. (4) as:

$$\hat{\mathbf{x}} = \sum_{i=0}^{I} \alpha_i \left(\mathcal{G}^H(\mathbf{x}_u) \mathbf{A}^H \mathbf{A} \mathcal{G}(\mathbf{x}_u) + \lambda \mathbf{I} \right) \mathbf{p}_i.$$
 (6)

Note that α_i and \mathbf{p}_i also depend on the motion estimation network $\mathcal{G}(\mathbf{x}_u)$ (refer to Alg. 1) which in turn depends on the trainable parameters θ .

Finally, we define our loss function \mathcal{L}_r as the mean squared error between the reconstruction estimation $\hat{\mathbf{x}}$ and the reference reconstruction target \mathbf{x}_{ref} . Thus, the final learning-based optimization function can be represented as:

$$\mathcal{L}_r = \left\| \sum_{i=0}^{I} \alpha_i \left(\mathcal{G}^H(\mathbf{x}_u) \mathbf{A}^H \mathbf{A} \mathcal{G}(\mathbf{x}_u) + \lambda \mathbf{I} \right) \mathbf{p}_i - \mathbf{x}_{ref} \right\|_2^2. \quad (7)$$

Now, the complete deep-learning forward chain is established and θ can be updated by gradient back-propagation. An end-to-end MCMR framework is cast without employing any intermediate motion-warping loss. In this respect, the motion estimation process is directly guided and driven by feedback from the final reconstruction performance but not by the motion estimation/registration. The goal of motion compensation is now aligned with the final reconstruction goal.

Algorithm 1 Algorithm of Conjugate Gradient

```
1: \mathbf{r}_0 := \mathbf{b}, \mathbf{x}_0 = \mathbf{0} \triangleright \mathbf{r} is the residual

2: \mathbf{p}_0 := \mathbf{r}_0, i := 0

3: while i < I do

4: \alpha_i := (\mathbf{r}_i^H \mathbf{r}_i / ((\mathbf{p}_i)^H \mathcal{V} \mathbf{p}_i))

5: \mathbf{x}_{i+1} := \mathbf{x}_i + \alpha_i \mathbf{p}_i

6: \mathbf{r}_{i+1} := \mathbf{r}_i - \alpha_i \mathcal{V} \mathbf{p}_i

7: \beta_i := (\mathbf{r}_{i+1})^H \mathbf{r}_{i+1} / ((\mathbf{r}_{i+1})^H \mathbf{r}_i)

8: \mathbf{p}_{i+1} := \mathbf{r}_{i+1} + \beta_i \mathbf{p}_i

9: i := i+1

10: end while
```

IV. EXPERIMENTS

A. Dataset and Implementation Details

43 subjects (27 patients and 16 healthy volunteers) were scanned with a 2D cardiac CINE sequence. The data is acquired in-house on a 1.5T MRI scanner (Magnetom Aera, Siemens Healthineers) with an acquisition sequence of 2D balanced steady-state free precession (bSSFP) equipped with multi-channel body and spine coil resulting in 30, 34 and 38 MR receiver coil channels. A $2\times$ GRAPPA acceleration generated the CINE data with an in-plane resolution of 1.9×1.9 mm², a slice thickness of 8mm, echo time (TE) of 1.06ms, and repetition time (TR) of 2.12ms. Retrospective gating is

used to bin the data into 25 cardiac phases with a temporal resolution of 40ms. Matrix size varies from the smallest size 176 (frequency-encoding) \times 132 (phase-encoding) to the largest size 192 \times 192. A stack of 10 to 15 slices for each subject along the long axis was acquired from base to apex under multiple breath-holds (2 slices per breath-hold). Slices without clear cardiac anatomy were discarded, resulting in a total of 366 cardiac motion-resolved image sequences. Retrospective undersampling is performed by Cartesian VISTA [38] sampling with varying acceleration factors.

The proposed framework was implemented in PyTorch (v1.9.0) and trained on an NVIDIA A40 GPU. The AdamW [39] optimizer combined with a one-cycle learning rate scheduler (max. learning rate 0.0001) was used to optimize Eq. (7). The network parameters for the *Motion Estimation Block* follows [24] and the hyper-parameters K, λ and I are set to 9, 0.01 and 10 for training and test. Regarding network training, we adopt either a fixed undersampling rate for training or a mixed training procedure with R=8, R=12, R=16 and R=20 undersampled data with a random selection with the same probability (dubbed as mixed R training). During inference, we test our approach on an arbitrary undersampling rate. The undersampled raw k-space data is first reconstructed by the *Reconstruction Initialization* block and then fed to the proposed network.

B. Ablation study

We investigate the benefits of using Eq. (7) as the loss function in comparison to the widely used motion-warping loss \mathcal{L}_w (refer to III-A) which breaks the MCMR into two sub-tasks for the MCMR reconstruction. To this respect, we conduct a set of experiments in which 4 trainings are carried out: 1. training only uses \mathcal{L}_r (Eq. (7)); 2. training only uses \mathcal{L}_w ; And we use a combined loss function $\mathcal{L} = \alpha \mathcal{L}_r + \beta \mathcal{L}_w$ only for this ablation study. We conduct the 3. training with $\alpha = 100, \beta = 1$ and 4. training with $\alpha = 10, \beta = 1$. We use reference images instead of the undersampled images in \mathcal{L}_w during the network training as proposed by [22], [34] to mitigate being affected by aliasing artifacts. All of these 4 experiments are trained and tested on R = 12.

We further investigate the impact of using different amounts of neighboring frames K for the dynamic CINE reconstruction during training and test. In the ideal case, the motion across the whole cardiac cycle can be estimated precisely, therefore all N temporal frames should be used to exploit the temporal redundancy. However, non-rigid contraction and expansion of the heart are challenging to estimate and given the 2D acquisition nature through-plane motion and occlusion (especially towards basal slices) can occur. Thus, the residual frame-toframe warping error cannot be suppressed completely to zero even with SOTA motion estimators. The more neighboring frames considered, the larger the accumulated residual motion error can occur. We therefore investigate the optimal number of neighboring frames to use for the CINE reconstruction. We run experiments using neighbouring $k=\pm 1$ (K=3), ± 2 , $\pm 4, \pm 6, \pm 8, \pm 12$ (K = 25) frames with mixed R training and test on different acceleration rates.

TABLE I

The impact of using end-to-end training with loss \mathcal{L}_r and the motion-warping loss \mathcal{L}_w with training on R=12 and test on R=16 accelerated data. PSNR is employed here as the evaluation metric. The failed training is marked with 'N.A.'.

Metric	only \mathcal{L}_r	α=100,β=1	α=10,β=1	only \mathcal{L}_w
PSNR	30.00	29.69	29.39	N.A.

Finally in order to test the method's generalizability, we implement a 5-fold cross-validation (35 subjects for training and 8 for testing). We repeat the experiments five times with the same parameter settings.

C. Baseline comparisons

We compare our method with six baseline methods. Two SOTA MCMR methods are considered in which the cardiac motion is estimated explicitly prior to the reconstruction. One is GRAFT-Recon [24], which applies GRAFT to predict the cardiac motion by using \mathcal{L}_w loss and then conducts the followup reconstruction task separately. The second one is Unrolled-MCMR [34], which performs an iterative unrolled joint optimization of cardiac motion estimation and reconstruction but its motion is also calculated from \mathcal{L}_w . Moreover, CG-SENSE [36], L+S [6], MoDL [40] and CTF-Net [12] are adopted as non-MCMR reconstruction methods for comparison. L+S solves the reconstruction by leveraging the decomposed low-rank and sparse matrix, MoDL uses an unrolled scheme with a dealiasing network and a data-consistency term, while CTF-Net tackles the problem by exploiting the k-tdomain redundancy using recurrent networks.

D. Evaluation

We apply Structural Similarity Index (SSIM) [41], Peak Signal-to-Noise Ratio (PSNR) and Normalized Mean Squared Error (NMSE) to evaluate the reconstruction performance quantitatively. Besides these three metrics, we also employ Learned Perceptual Image Patch Similarity (LPIPS) [42] which has been verified to be closer to human perception. Furthermore, we use a cardiac segmentation network [43] to obtain a bounding box around the heart to focus evaluation on the cardiac anatomy. An offset value of 10 pixels is set to extend the bounding box region. All metrics (SSIM, PSNR, NMSE and LPIPS) are evaluated within this heart region.

V. RESULTS

A. Ablation Study

We foremost delve into the ablation study to find out the best training setting for our proposed approach. The final training performance is shown in Table I. It can be seen that the more \mathcal{L}_w participates in the training, the worse the reconstruction quality becomes. The training fails (does not converge) if only \mathcal{L}_w is used since the undersampled R=12 images differ from the reference images severely and the motion network cannot find a correlation between them.

The quantitative evaluation for the optimal amount of neighboring frames is shown in Table II. A qualitative analysis of

TABLE II

The reconstruction performance of using different neighboring frames amount K. PSNR is employed here as the evaluation metric and calculated on the whole range of images. The top two results are marked in bold.

K	R = 8	R = 12	R = 16	R = 20
3	40.79 ± 2.25	37.31 ± 2.09	33.14 ± 2.44	29.52 ± 2.69
5 9	42.39 ± 2.82 41.27 ± 3.74	39.73 ± 2.32 39.85 ± 3.03	36.73 ± 2.03 38.26 ± 2.57	33.64 ± 2.97 36.58 ± 2.76
13 17	40.20 ± 3.72 39.31 ± 3.31	39.16 ± 3.38 38.46 ± 3.21	37.92 ± 3.02 37.33 ± 3.01	36.95 ± 2.83 36.61 ± 2.99
25	37.99 ± 2.85	37.26 ± 2.77	36.21 ± 2.69	35.77 ± 2.90

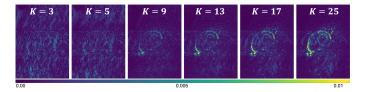


Fig. 3. Reconstruction error maps between reconstructed and reference image for using different neighboring frames amount K on a test sample with acceleration rate R=20.

the reconstruction error for the R=20 case is illustrated in Fig. 3. It can be seen that adopting fewer neighboring frames in low acceleration rates is preferable. Yet with the increase of acceleration rate for a small number of neighboring frames, no sufficient temporal redundancy is captured, resulting in increased reconstruction errors in the image background as shown in the $K=3(\pm 1)$ and $5(\pm 2)$ cases. However, if a high number of neighboring frames is chosen, a performance drop is observed because the advantage of using more redundant information from other frames is overcome by the suboptimal large and through-plane motion errors. In this case, motionwarping errors accumulate around the heart region while the background error is suppressed (refer to the K=25 case). We found that choosing K = 9 is an optimal trade-off across all acceleration rates as indicated in Table II. Therefore, we applied this value for the reconstruction in all experiments.

For the evaluation of the generalization, the averaged PSNR and SSIM across the 5 folds are displayed in Table III. Regarding both PSNR and SSIM metrics, the performance difference between these 5 folds is smaller than the standard deviation within one specific fold. Therefore, we can conclude that the proposed method demonstrates robust behavior toward subject domain shifts.

TABLE III 5 FOLD CROSS-VALIDATION OF THE PROPOSED NETWORK WITH MIXED R TRAINING AND TEST ON R=8 AND R=16 Cases. PSNR and SSIM VALUES ARE SHOWN.

Fold	R =	= 8	R = 16		
	PSNR	SSIM	PSNR	SSIM	
Fold 1 Fold 2 Fold 3 Fold 4 Fold 5 Avg.	31.57 ± 5.38 31.45 ± 4.04 32.81 ± 5.00 32.42 ± 3.22 31.59 ± 3.46 31.96 ± 4.28	0.92 ± 0.04 0.92 ± 0.04 0.93 ± 0.04 0.93 ± 0.03 0.93 ± 0.04 0.93 ± 0.04	28.88 ± 3.98 29.22 ± 3.86 30.42 ± 4.09 30.16 ± 3.12 29.40 ± 3.24 29.66 ± 3.69	0.87 ± 0.06 0.88 ± 0.06 0.89 ± 0.06 0.89 ± 0.05 0.89 ± 0.05 0.88 ± 0.06	

TABLE IV

QUANTITATIVE COMPARISON OF THE PROPOSED FRAMEWORK, CG-SENSE [36], L+S [6], MODL [40], CTF-NET [12], GRAFT-RECON [24] AND UNROLLED-MCMR [34] DURING INFERENCE FOR R=8, 12, 16 AND R=20. PEAK SIGNAL TO NOISE RATIO (PSNR), STRUCTURE SIMILARITY (SSIM), LEARNED PERCEPTUAL IMAGE PATCH SIMILARITY (LPIPS) AND NORMALIZED MEAN SQUARED ERROR (NMSE) ARE ADOPTED AS EVALUATION METRICS AND THEIR AVERAGED VALUE WITH CORRESPONDING STANDARD DEVIATION ACROSS ALL TEST SAMPLES ARE SHOWN. METHODS' AVERAGE EXECUTION TIME OF RECONSTRUCTING THE SAMPLE WITH SPATIAL RESOLUTION 192×156 IS LOGGED. THE BEST RESULTS ARE MARKED IN BOLD.

	Metrics	CG-SENSE	L+S	MoDL	CTF-Net	GRAFT-Recon	Unrolled-MCMR	Proposed
R=8	PSNR	23.88 ± 2.01	26.40 ± 2.11	28.80 ± 2.04	27.41 ± 2.80	29.02 ± 3.08	30.46 ± 6.23	31.57 ± 5.38
	SSIM	0.76 ± 0.05	0.84 ± 0.04	0.88 ± 0.03	0.88 ± 0.05	0.89 ± 0.05	0.90 ± 0.05	$\textbf{0.92}\pm\textbf{0.04}$
	LPIPS	0.08 ± 0.03	0.06 ± 0.02	0.02 ± 0.01	0.04 ± 0.02	0.03 ± 0.02	0.03 ± 0.02	$\textbf{0.02}\pm\textbf{0.01}$
	NMSE	0.25 ± 0.06	0.18 ± 0.04	0.14 ± 0.03	0.16 ± 0.05	0.14 ± 0.05	0.13 ± 0.05	$\textbf{0.11}\pm\textbf{0.05}$
R = 12	PSNR	17.54 ± 2.47	20.87 ± 2.65	22.05 ± 2.78	25.27 ± 2.64	25.19 ± 2.53	29.41 ± 4.76	30.10 ± 4.38
	SSIM	0.51 ± 0.09	0.70 ± 0.07	0.70 ± 0.08	0.84 ± 0.05	0.80 ± 0.07	0.88 ± 0.06	0.89 ± 0.05
	LPIPS	0.18 ± 0.06	0.09 ± 0.04	0.08 ± 0.04	0.05 ± 0.03	0.07 ± 0.05	0.03 ± 0.02	$\textbf{0.02}\pm\textbf{0.01}$
	NMSE	0.52 ± 0.13	0.34 ± 0.08	0.31 ± 0.09	0.20 ± 0.05	0.21 ± 0.06	0.14 ± 0.06	$\textbf{0.13}\pm\textbf{0.05}$
R = 16	PSNR	15.09 ± 2.53	16.81 ± 2.96	17.22 ± 3.40	23.67 ± 2.62	23.55 ± 2.44	28.44 ± 4.20	28.88 ± 3.98
	SSIM	0.35 ± 0.12	0.50 ± 0.13	0.47 ± 0.14	0.80 ± 0.06	0.73 ± 0.08	0.86 ± 0.07	$\textbf{0.87}\pm\textbf{0.06}$
	LPIPS	0.24 ± 0.07	0.16 ± 0.06	0.16 ± 0.07	0.07 ± 0.03	0.11 ± 0.06	0.03 ± 0.02	0.03 ± 0.02
	NMSE	0.69 ± 0.17	0.54 ± 0.15	0.54 ± 0.19	0.23 ± 0.06	0.26 ± 0.07	0.15 ± 0.06	$\textbf{0.15}\pm\textbf{0.06}$
R = 20	PSNR	14.24 ± 2.44	15.27 ± 2.77	15.43 ± 3.23	23.37 ± 2.68	22.66 ± 2.52	27.71 ± 3.95	27.90 ± 3.81
	SSIM	0.29 ± 0.11	0.39 ± 0.13	0.36 ± 0.14	0.78 ± 0.07	0.68 ± 0.09	0.84 ± 0.08	$\textbf{0.85}\pm\textbf{0.07}$
	LPIPS	0.26 ± 0.07	0.20 ± 0.06	0.21 ± 0.08	0.08 ± 0.04	0.13 ± 0.08	0.05 ± 0.03	0.04 ± 0.03
	NMSE	0.75 ± 0.17	0.64 ± 0.16	0.65 ± 0.19	0.25 ± 0.06	0.29 ± 0.08	$\textbf{0.17}\pm\textbf{0.07}$	$\textbf{0.17}\pm\textbf{0.07}$
Avg. Time (s)		$\textbf{0.29}\pm\textbf{0.01}$	1.73 ± 0.01	2.48 ± 0.01	3.00 ± 0.01	5.37 ± 0.01	14.89 ± 0.03	5.49 ± 0.01

B. Baseline comparisons

We compare our method to six baseline methods (see IV-C). The deep learning approaches included the proposed network, MoDL [40] and CTF-Net [12] are trained with mixed Rtraining procedure (see IV-A). These methods can achieve their best performance by using this training procedure. The mixed R training procedure is not applied to GRAFT-Recon [24] and Unrolled-MCMR [34] since including highly undersampled data gave rise to unstable training and poor reconstruction performance. In practice we found that GRAFT-Recon can achieve the best inference results when using the fixed R=8training compared to all other fixed R trainings. For Unrolled-MCMR, the fixed R = 12 training is the best training strategy. Thus, for GRAFT-Recon a fixed R=8 training is conducted, while for Unrolled-MCMR training we only use R = 12 data. Besides, we also set their temporal neighborhood to K=9with ± 4 neighboring frames, whilst in their original work they employed all temporal frames which can cause higher warping errors. After training, all six methods are tested on an arbitrary undersampling rate. The quantitative performance evaluated by metrics PSNR, NMSE, SSIM, and LPIPS is shown in Table IV.

The superior and consistent performance of the proposed method is shown across every single undersampling rate compared to all other baseline methods and regardless of the evaluation metric. It can be noted that learning-based methods e.g. GRAFT-Recon, Unrolled-MCMR, CTF-Net and MoDL outperform conventional methods like CG-SENSE and L+S. Moreover, Unrolled-MCMR consistently demonstrates the second-best performance because of its usage of reference images in the motion-warping loss function and its unrolled iterative optimization mechanism. The advantage of iterative optimization becomes more prominent for higher acceleration rates.

The qualitative comparison of two test subjects (healthy subject and patient) between the proposed network and the non-MCMR methods is illustrated in Fig. 4 for undersampling rates of R=8 and R=16. The corresponding error maps are displayed as well. The proposed network presents a consistent performance in both subjects with the highest PSNR score and lowest residual error. Temporal traces are in good agreement with the fully-sampled reference and cardiac dynamics were recovered by the proposed network. Diagnostic features like papillary muscles are restored clearly without blurring in both cases. Moreover, it is apparent that MoDL does not leverage any temporal information to reconstruct the cardiac frames. While CTF-Net and MoDL still show comparable results for R=8, a severe performance drop for MoDL is perceived in R=16. The same conclusion can also be drawn from Table IV. This indicates the importance of leveraging temporal redundancy during the reconstruction, especially in highly accelerated cases.

Further qualitative comparison of two test subjects (healthy subject and patient) between the proposed framework and other MCMR methods (GRAFT-Recon and Unrolled-MCMR) are demonstrated in Fig. 5. The proposed network outperforms the two compared MCMR methods in both R=12 and R=20. While the proposed framework is only trained with one loss term (without any smoothness terms), it predicts a more meaningful and dense motion field even for R=20. The motion estimation from Unrolled-MCMR is sparse and non-smooth, in spite of the usage of smoothness terms during training. The GRAFT-Recon reveals inferior reconstruction due to the motion estimation being artifact-affected resulting in error propagation amongst frames, while the proposed method yields a reconstruction image without any aliasing in both cardiac region and background.

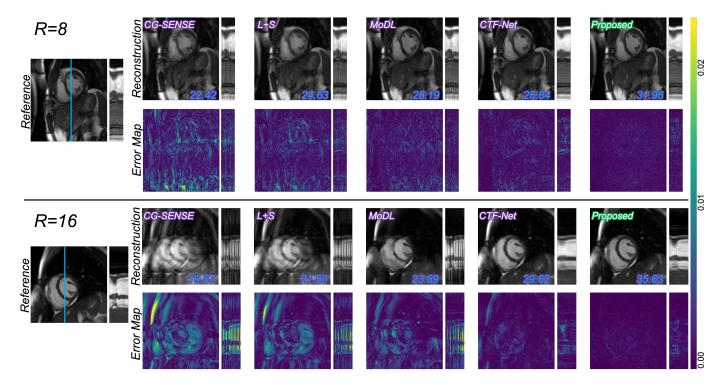


Fig. 4. Qualitative comparison of the proposed method to non-MCMR methods including CG-SENSE [36], L+S [6], MoDL [40] and CTF-Net [12] in the R=8 (patient with myocarditis) and R=16 (healthy subject) accelerated acquisition. The respective PSNR values of the heart region are depicted in the image. Reference images, reconstructed images and their corresponding error maps are demonstrated. The spatial (x-y) images are depicted next to the temporal traces (y-t) through the middle of the left ventricle. The selected y-axis is marked with a blue line in the reference image.

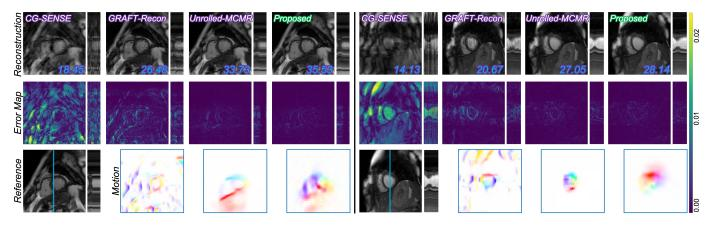


Fig. 5. Qualitative comparison of the proposed network to CG-SENSE [36], GRAFT-Recon [24] and Unrolled-MCMR [34] in the R=12 (left side, healthy subject) and R=20 (right side, patient with myocarditis) accelerated acquisition. The respective PSNR values of the heart region are shown in the image. Reference images, reconstructed images, corresponding error maps and color-wheel-encoded [44] motion field visualization are shown. The spatial (x-y) images are depicted next to the temporal traces (y-t) through the left ventricle. The selected y-axis is marked with a blue line in the reference image.

VI. DISCUSSION

MCMR is a powerful and straightforward concept that has been demonstrated for the reconstruction of cardiac CINE [25], [33], [34], [45]. However, a wide range of MCMR implementations for CINE is precluded by two major unsolved challenges: high-speed MCMR processing and precise artifact-suppressed cardiac motion estimation. In this work, we proposed a learning-based MCMR framework for CINE imaging that copes with these two problems at once. The fast MCMR is achieved by leveraging the trained network to accelerate the estimation process in inference time, whilst the artifact-suppressed motion estimation is achieved using reconstruction-

driven motion estimation. We treat the two sub-tasks as a single entity, in which the training loss is back-propagated end-to-end from the final reconstructed images to the motion estimation input.

We performed an ablation study in which the use of an intermediate warping similarity loss is compared to a final reconstruction loss. Results indicate that if the optimization is driven by the final reconstruction loss, not only the reconstruction performance is enhanced, but also the motion prediction is ameliorated. Furthermore, we investigated the aspect of the optimal number of neighboring frames in the cardiac cycle to be used for MCMR. The conducted experiments

demonstrate that the higher the acceleration rate, the more neighboring frames are preferable. There is a trade-off between the static reconstruction error which is incurred by the lack of redundant information, and the dynamic reconstruction error around the heart which is caused by residual warping errors from neighboring frames. It is important to note that this phenomenon is not only occurring in our proposed approach but is generic for any MCMR method. Based on these results, we set a fixed number of neighboring frames in this work. In the future, we plan to make this important hyper-parameter learnable so it can self-adapt to the optimal value for different application scenarios.

We further conduct a systematic analysis of the proposed approach compared to baseline methods. The consistent and superior performance of our proposed method is found throughout this work. We conclude from the experiments that learningbased methods usually outperform non-learning-based methods. Furthermore, methods that leverage the whole cardiac cycle e.g. CTF-Net usually outperform methods that leverage less temporal redundancy e.g. MoDL, especially in the high acceleration case. Furthermore, Unrolled-MCMR showed similar but inferior performance results to the proposed method. This is attributed to two major reasons. First, we carry out just a single but more effective optimization instead of applying alternating updates of motion fields and image reconstructions. It should be noted that our proposed method can also be extended as an iterative unrolled optimization but at the cost of prolonged training and test time. Second, we only have one simple reconstruction loss term \mathcal{L}_r in the final stage, while Unrolled-MCMR employs a conventional motion-warping loss \mathcal{L}_w together with two regularization terms, requiring nontrivial weighting factor tuning.

The superior results of the proposed method can be attributed to the artifact-suppressed motion estimation (refer to the motion fields in Fig. 5). The proposed *Motion-Compensated Reconstruction Block* can be regarded as a transformation operator which extends the motion estimation procedure from image space to k-space. Although Eq. (7) presents a loss function that forces the framework to generate a reference resembled reconstruction, it can also be interpreted as a warping loss function which warps a set of undersampled images by the estimated motion to the target images while ensuring consistency to acquired k-space samples.

Furthermore, our proposed approach provides another perspective on solving the cardiac motion estimation/registration problem. Cardiac motion estimation/registration can not only be used inside the MCMR framework for reconstruction but can also be applied for cardiac feature tracking to evaluate myocardial strain and functional analysis [46], [47] or to facilitate cardiac segmentation tasks [48]. Our proposed method can be recast to a motion estimation/registration method with two major benefits compared to the conventional motion estimation/registration methods. First, we only need a single loss term (Eq. (7)) to generate smooth and realistic motion fields avoiding further hyper-parameter tuning. Second, we can predict high-quality cardiac motion directly from highly-undersampled MR data. It is also conceivable that we do not need visually appealing MR images for the extraction

and quantification of clinical parameters (e.g. left ventricular function). A potential synergistic approach for jointly reconstructing, analyzing (e.g. segmentation or motion tracking) and interpreting the cardiac CINE imaging will be developed further based on this study.

In the end, we also acknowledge some limitations of our work. First, the motion estimation is based on the backbone of GRAFT. It conducts $N \times K$ computations to reconstruct the cardiac cycle with N frames which are suboptimal regarding estimation speed and memory usage. In future work, we will attempt to build a more efficient and lightweight group-wise motion estimator to accelerate the reconstruction process further. Moreover, currently our MCMR framework only learns motion prediction and uses only one non-learnable regularizer. This has been proven in this work as a simple yet effective approach, but we have not yet integrated our motion estimates in learnable denoising regularizers [40], [49], which will be subject to future work. Finally, the proposed work is solely evaluated for retrospective undersampling. The test performance on a larger cohort including prospectively collected data will also be evaluated in future work.

VII. CONCLUSION

In this work, we proposed a learning-based MCMR framework for CINE imaging. We introduce a mechanism that solves the MCMR problem as a single entity and drives the motion estimation directly from the final reconstruction perspective. The training loss is back-propagated through the whole pipeline and the framework is optimized end-to-end without breaking into two sub-tasks. We find out that using a smaller neighboring frames number to conduct MCMR can achieve better results than using all sequence frames. Our method shows consistent performance throughout all conducted experiments and outperforms all baseline methods. We have confidence that the developed method for cardiac CINE imaging can also be generalized and applied to other reconstruction applications.

REFERENCES

- [1] P. Kellman, F. H. Epstein, and E. R. McVeigh, "Adaptive sensitivity encoding incorporating temporal filtering (tsense)†," *Magnetic Resonance in Medicine*, vol. 45, no. 5, pp. 846–852, 2001. [Online]. Available: https://onlinelibrary.wiley.com/doi/abs/10.1002/mrm.1113
- [2] F. A. Breuer, P. Kellman, M. A. Griswold, and P. M. Jakob, "Dynamic autocalibrated parallel imaging using temporal grappa (tgrappa)," *Magnetic Resonance in Medicine*, vol. 53, no. 4, pp. 981–985, 2005. [Online]. Available: https://onlinelibrary.wiley.com/doi/abs/10.1002/mrm.20430
- [3] H. Jung, K. Sung, K. S. Nayak, E. Y. Kim, and Y. J. C., "k-t focuss: A general compressed sensing framework for high resolution dynamic mri," *Magnetic Resonance in Medicine*, vol. 61, no. 1, pp. 103–116, 2009.
- [4] R. Otazo, D. Kim, L. Axel, and D. K. Sodickson, "Combination of compressed sensing and parallel imaging for highly accelerated first-pass cardiac perfusion mri," *Magnetic Resonance in Medicine*, vol. 64, no. 3, pp. 767–776, 2010. [Online]. Available: https://onlinelibrary.wiley.com/doi/abs/10.1002/mrm.22463
- [5] P. G. Batchelor, D. Atkinson, P. Irarrazaval, D. L. G. Hill, H. J., and L. D., "Matrix description of general motion correction applied to multishot images," *Magnetic Resonance in Medicine*, vol. 54, p. 1273–1280, 2005.

- [6] R. Otazo, E. Candès, and D. K. Sodickson, "Low-rank plus sparse matrix decomposition for accelerated dynamic mri with separation of background and dynamic components," *Magnetic Resonance in Medicine*, vol. 73, no. 3, pp. 1125–1136, 2015. [Online]. Available: https://onlinelibrary.wiley.com/doi/abs/10.1002/mrm.25240
- [7] W. Huang and et al., "Deep low-rank plus sparse network for dynamic mr imaging," *Medical Image Analysis*, vol. 73, p. 102190, 2021.
- [8] T. Küstner, N. Fuin, K. Hammernik, and et al., "CINENet: deep learning-based 3D cardiac CINE MRI reconstruction with multi-coil complex-valued 4D spatio-temporal convolutions," *Scientific Reports*, vol. 10, no. 1, pp. 1–13, 2020.
- [9] C. M. Sandino, P. Lai, S. S. Vasanawala, and J. Y. Cheng, "Accelerating cardiac cine mri using a deep learning-based espirit reconstruction," *Magnetic Resonance in Medicine*, vol. 85, no. 1, 2021.
- [10] S. G. Lingala, Y. Hu, E. DiBella, and M. Jacob, "Accelerated dynamic mri exploiting sparsity and low-rank structure: k-t slr," *IEEE Transac*tions on Medical Imaging, vol. 30, no. 5, pp. 1042–1054, 2011.
- [11] C. Qin and et al., "k-t next: Dynamic mr image reconstruction exploiting spatio-temporal correlations," in *Medical Image Computing and Com*puter Assisted Intervention, 2019, pp. 505–513.
- [12] —, "Complementary time-frequency domain networks for dynamic parallel mr image reconstruction," *Magnetic Resonance in Medicine*, vol. 86, no. 6, pp. 3274–3291, 2021.
- [13] S. Klein, M. Staring, K. Murphy, and J. Pluim, "Elastix: a toolbox for intensity-based medical image registration," *IEEE Transactions on Medical Imaging*, vol. 29, no. 1, pp. 196–205, 2009.
- [14] M. Modat and et al., "Fast free-form deformation using graphics processing units," *Computer Methods and Programs in Biomedicine*, vol. 98, no. 3, pp. 278–284, 2010.
- [15] T. Vercauteren, X. Pennec, A. Perchant, and N. Ayache, "Diffeomorphic demons: Efficient non-parametric image registration," *Neuro Image*, vol. 45, no. 1, pp. S61–S72, 2009.
- [16] X. Chen, A. Diaz-Pinto, N. Ravikumar, and A. F. Frangi, "Deep learning in medical image registration," *Progress in Biomedical Engineering*, vol. 3, no. 1, p. 012003, feb 2021. [Online]. Available: https://dx.doi.org/10.1088/2516-1091/abd37c
- [17] G. Balakrishnan, A. Zhao, M. R. Sabuncu, J. Guttag, and A. Dalca, "An unsupervised learning model for deformable medical image registration," in 2018 IEEE/CVF Conference on Computer Vision and Pattern Recognition, 2018, pp. 9252–9260.
- [18] ——, "Voxelmorph: A learning framework for deformable medical image registration," *IEEE Transactions on Medical Imaging*, vol. 38, no. 8, pp. 1788–1800, 2019.
- [19] M. A. Morales, D. Izquierdo-Garcia, I. Aganj, J. Kalpathy-Cramer, B. R. Rosen, and C. Catana, "Implementation and validation of a threedimensional cardiac motion estimation network." in *Radiol Artificial Intelligence*, vol. 4, no. 1, 2019.
- [20] H. Yu, X. Chen, H. Shi, T. Chen, T. S. Huang, and S. Sun, "Motion pyramid networks for accurate and efficient cardiac motion estimation," *CoRR*, vol. abs/2006.15710, 2020.
- [21] J. Pan, D. Rueckert, T. Küstner, and K. Hammernik, "Efficient image registration network for non-rigid cardiac motion estimation," in *Ma-chine Learning for Medical Image Reconstruction*, 2021, pp. 14–24.
- [22] H. Qi and et al., "End-to-end deep learning nonrigid motion-corrected reconstruction for highly accelerated free-breathing coronary mra," Magnetic Resonance in Medicine, vol. 86, no. 1, pp. 1983–1996, 2021.
- [23] T. Küstner and et al., "Lapnet: Non-rigid registration derived in k-space for magnetic resonance imaging," *IEEE Transactions on Medical Imaging*, vol. 40, no. 12, pp. 3686–3697, 2021.
- [24] K. Hammernik, J. Pan, D. Rueckert, and T. Küstner, "Motion-guided physics-based learning for cardiac mri reconstruction," Asilomar Conference on Signals, Systems, and Computers, 2021.
- [25] J. Yang, T. Küstner, P. Hu, P. Liò, and H. Qi, "End-to-end deep learning of non-rigid groupwise registration and reconstruction of dynamic mri," *Frontiers in Cardiovascular Medicine*, vol. 9, 2022. [Online]. Available: https://www.frontiersin.org/articles/10.3389/fcvm.2022.880186
- [26] G. Cruz, D. Atkinson, M. Henningsson, R. Botnar, and C. Prieto, "Highly efficient nonrigid motion-corrected 3d whole-heart coronary vessel wall imaging," *Magnetic Resonance in Medicine*, vol. 77, no. 5, pp. 1894–1908, 2017.
- [27] A. Bustin and et al., "3d whole-heart isotropic sub-millimeter resolution coronary magnetic resonance angiography with non-rigid motion-compensated prost," *Journal of Cardiovascular Magnetic Resonance*, vol. 22, no. 1, 2020.
- [28] F. Odille, P. A. Vuissoz, P. Y. Marie, and J. Felblinger, "Generalized reconstruction by inversion of coupled systems (grics) applied to free-

- breathing mri," Magnetic Resonance in Medicine, vol. 60, pp. 146–157, 2008
- [29] F. Odille and et al., "Joint reconstruction of multiple images and motion in mri: Application to free-breathing myocardial t₂ quantification," *IEEE Transactions on Medical Imaging*, vol. 35, no. 1, pp. 197–207, 2016.
- [30] J. Royuela-del Val, L. Cordero-Grande, F. Simmross-Wattenberg, M. Martín-Fernández, and C. Alberola-López, "Nonrigid groupwise registration for motion estimation and compensation in compressed sensing reconstruction of breath-hold cardiac cine mri," *Magnetic Resonance in Medicine*, vol. 75, no. 4, pp. 1525–1536, 2016. [Online]. Available: https://onlinelibrary.wiley.com/doi/abs/10.1002/mrm.25733
- [31] N. Zhao, D. O'Connor, A. Basarab, D. Ruan, and K. Sheng, "Motion compensated dynamic mri reconstruction with local affine optical flow estimation," *IEEE Transactions on Biomedical Engineering*, vol. 66, no. 11, pp. 3050–3059, 2019.
- [32] A. I. Aviles-Rivero, N. Debroux, G. Williams, M. J. Graves, and C. Schönlieb, "Compressed sensing plus motion (cs + m): A new perspective for improving undersampled mr image reconstruction," *Medical Image Analysis*, vol. 68, p. 101933, 2021.
- [33] T. Schmoderer, A. I. Aviles-Rivero, V. Corona, N. Debroux, and C. Schönlieb, "Learning optical flow for fast MRI reconstruction," *Inverse Problems*, vol. 37, no. 9, p. 095007, aug 2021.
- [34] J. Pan, D. Rueckert, T. Küstner, and K. Hammernik, "Learning-based and unrolled motion-compensated reconstruction for cardiac mr cine imaging," in *Medical Image Computing and Computer Assisted Inter*vention, 2022, pp. 686–696.
- [35] T. Küstner and et al., "Deep-learning based motion-corrected image reconstruction in 4d magnetic resonance imaging of the body trunk," in 2020 Asia-Pacific Signal and Information Processing Association Annual Summit and Conference (APSIPA ASC), 2020, pp. 976–985.
- [36] K. P. Pruessmann, M. Weiger, P. Börnert, and P. Boesiger, "Advances in sensitivity encoding with arbitrary k-space trajectories," *Magnetic Resonance in Medicine*, no. 46, pp. 638–651, 2001.
- [37] W. H. Press, S. A. Teukolsky, W. T. Vetterling, and B. P. Flannery, Numerical Recipes in C, 2nd ed. Cambridge, USA: Cambridge University Press, 1992.
- [38] R. Ahmad, H. Xue, S. Giri, Y. Ding, J. Craft, and O. P. Simonetti, "Variable density incoherent spatiotemporal acquisition (vista) for highly accelerated cardiac mri," *Magnetic Resonance in Medicine*, vol. 74, no. 5, pp. 1266–1278, 2015.
- [39] I. Loshchilov and F. Hutter, "Decoupled weight decay regularization," arXiv preprint arXiv:1711.05101, no. 19, 2017.
- [40] H. K. Aggarwal, M. P. Mani, and M. Jacob, "Model based image reconstruction using deep learned priors (modl)," in *IEEE International Symposium on Biomedical Imaging (ISBI)*, 2018, pp. 671–674.
- [41] Z. Wang, A. C. Bovik, H. R. Sheikh, and E. P. Simoncelli, "Image quality assessment: from error visibility to structural similarity," *IEEE Transaction of Image Process*, vol. 13, no. 4, pp. 600–612, 2004.
- [42] R. Zhang, P. Isola, A. A. Efros, E. Shechtman, and O. Wang, "The unreasonable effectiveness of deep features as a perceptual metric," in Conference on Computer Vision and Pattern Recognition, 2018.
- [43] C. Chen and et al., "Deep learning for cardiac image segmentation: A review," Frontiers in Cardiovascular Medicine, vol. 7, 2020. [Online]. Available: https://www.frontiersin.org/articles/10.3389/fcvm.2020.00025
- [44] S. Baker and et al., "A database and evaluation methodology for optical flow," in 2007 IEEE 11th International Conference on Computer Vision, 2007, pp. 1–8.
- [45] G. Cruz, K. Hammernik, T. Kuestner, D. Rueckert, R. Botnar, and C. Prieto, "One-heartbeat cardiac cine imaging via jointly regularized non-rigid motion corrected reconstruction," in *Proc. International Society for Magnetic Resonance in Medicine (ISMRM)*, 2021, p. 0070.
- [46] R. J. Taylor and et al., "Myocardial strain measurement with feature-tracking cardiovascular magnetic resonance: normal values," *European Heart Journal Cardiovascular Imaging*, vol. 16, no. 8, pp. 871–881, 02 2015. [Online]. Available: https://doi.org/10.1093/ehjci/jev006
- [47] G. Pedrizzetti, P. Claus, P. J. Kilner, and E. Nagel, "Principles of cardiovascular magnetic resonance feature tracking and echocardiographic speckle tracking for informed clinical use," *Journal of Cardiovascular Magnetic Resonance*, vol. 18, no. 1, p. 51, Aug 2016. [Online]. Available: https://doi.org/10.1186/s12968-016-0269-7
- [48] C. Qin and et al., "Joint learning of motion estimation and segmentation for cardiac mr image sequences," in *Medical Image Computing and Computer Assisted Intervention*, 2018.
- [49] K. Hammernik and et al., "Learning a variational network for reconstruction of accelerated mri data," *Magnetic Resonance in Medicine*, vol. 79, no. 6, pp. 3055–3071, 2018.